Dynamic stability identification using a scale mock-up of an advanced aircraft configuration

*Stefan BOGOS**
**INCAS-National Institute for Aerospace Research "Elie Carafoli"*
B-dul Iuliu Maniu 220, Bucharest 061126, Romania, bogos@incas.ro

Abstract
This paper deals with the stability of a real aircraft using the results from a flying scale mock-up. Similarity coherent criteria are proposed for the dimensional, inertial and mass characteristics between the two models. The flight condition preserves the lift coefficient. The same values for the damping factors are in "Short period" and "Dutch roll" modes. Factored values with a scale constant are obtained for the time characteristics in "Short period ", "Dutch roll", "Roll" and "Spiral" modes. The damping ratio in "Phugoid mode" seems to be proportional to the aerodynamic drag ratio of the two models.

1. Introduction

The aircraft stability analysis requests as input data, the aircraft mass, inertia and the detailed aerodynamic coefficients and derivatives. The classical assumptions for the general equations of the unsteady aircraft motion analysis imply: uncoupling "longitudinal" and "lateral", small perturbation and linear equations of the motion. Sometimes this theoretical hypothesis, together with an uncertainty on the input data, would produce unsatisfactory results for the longitudinal and lateral-directional flying qualities.
Airplanes must be designed to satisfy the Level 1 for Flying Quality requirements with all systems in their normal operating state. If, for an already built aircraft, after the first flight test program, an unsatisfactory stability has been recorded, important and expensive changes have to be done. The following example shows that British certification requirements relating to the Dutch roll damping in engine-out go-around, forced Boeing to increase the height of the tail fin on all 707 variants, as well as to add a ventral fin. A study about the effects of these modifications was detailed in [1].
The airplane model used in this study is an advanced aircraft configuration, developed for low drag and noise which has been proposed in the international European research program: HELENA-Highly Environmental Low Emission Next generation regional Aircraft. It has specific features: forward swept wings with winglets, twin vertical tails and Contra Rotating Open Rotors that are shielded by horizontal tail, fig.1.
This paper aims to achieve a study for increasing the quality of the results concerning the stability of this advanced aircraft configuration, using the results from a flying mock-up. The scale ratio of the scale mock-up related to the full aircraft was 1/20. The content of this report completes the topics from [2] and [3] and details how to translate the recorded stability parameters from a flying mock-up to the real aircraft.

2. The aerodynamic model

The following is a short presentation about a specific practical method regarding the evaluation of the pressure distribution on the outside surface of the aircraft. It is assumed that there is a general steady subsonic motion composed by a translation with $\vec{V}_\infty$ velocity and an aircraft rotation with angular velocity $\vec{\omega}(p,q,r)$. Also, a potential flow without viscous effects is assumed and there are accepted the "aerodynamics" approaches of the geometry according to "small perturbations". The potential theory is used to get the solution. The three-dimensional boundary value problem is solved using the "boundary element method", [7].
The "boundary element" method is a specific method, developed especially for differential equations of Laplace or Poisson type. The way to solve the potential equation is using singularities of the source type, vortices or doublets in

order to form the integral equation that describes the potential. The figure 1 is a representation of the aerodynamic mesh for HELENA aircraft model, "Full scale" that was used in this evaluation.

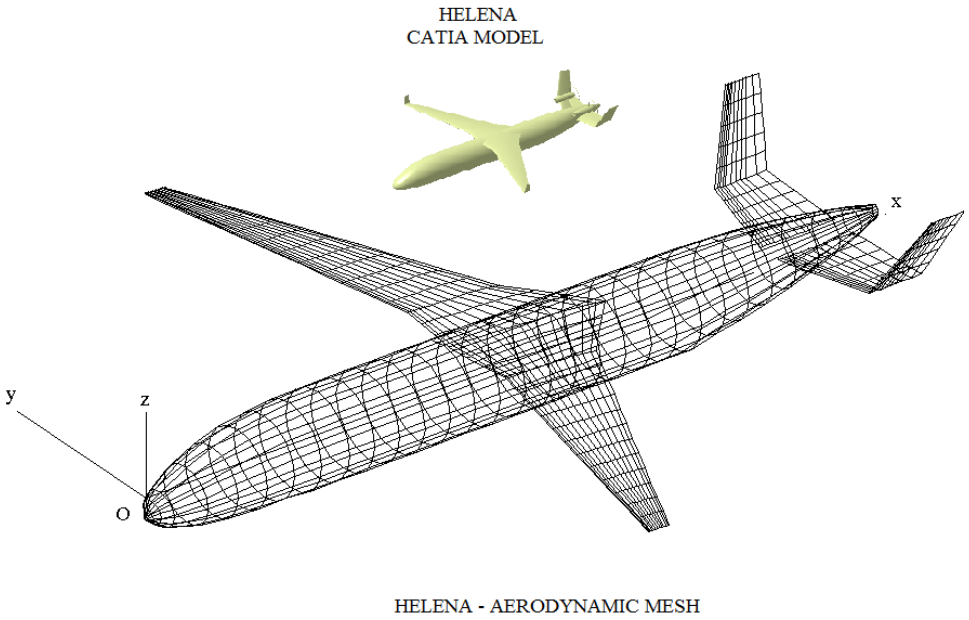

Fig. 1 HELENA: CATIA Model and Aerodynamic mesh, "Full Aircraft"

The forward swept wing, (FSW), is specific to the proposed configuration. Figure 2 shows a generic comparative analysis of the laminar flow surface (blue shaded area) on the forward swept wing and backward swept wing, (BSW), in flight cruise regime. Note that the laminar shaded area for forward swept wing is greater than the laminar shaded area for backward swept wing that has the effect of reducing the aerodynamic drag for FSW.

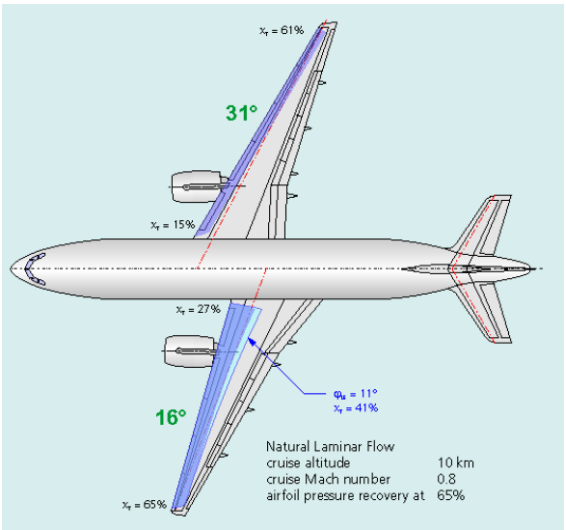

Fig.2 Natural laminar flow on swept wings, ref [11]

By using the Green theorem, we obtain that the potential ϕ in a point P, outside to the S surface of the aircraft, is given by the expression (1):

$$\phi(\mathrm{P}) = -\frac{1}{4\pi}\int_S \frac{1}{r(p,q)}\frac{\partial \phi}{\partial n}(q)\,dS + \frac{1}{4\pi}\int_S \phi(q)\frac{\partial}{\partial n}\left(\frac{1}{r(p,q)}\right)_q dS \qquad (1)$$

The boundary conditions described through equations (2), applied to the disturbance potential φ are as follows:

$$\begin{cases} \Delta\varphi = 0, on\ the\ outside\ S, region \\ \left(\dfrac{\partial\varphi}{\partial n}\right)_S = -\vec{n}\cdot\vec{V}_\infty, \quad on\ the\ body \\ \varphi = 0, \quad at\ \infty \end{cases} \tag{2}$$

Let $\sigma(q)$ be the intensity of a sources panel in a point q on the surface of the non-lifting body, or on the skeleton of the wing, and $\Gamma(k)$ the intensity of the circulation of a horseshoe vortex in the point k on the medium surface.
Conditions (2) and (1), applied to the specific singularities will give equation (3):

$$2\pi\sigma(p) - \int_S \frac{\partial}{\partial n_p}\left(\frac{1}{r(p,q)}\right)\sigma(q)ds + \frac{1}{4\pi}\vec{n}(p)\sum_{k=1}^{Nk}\int_{l_k}\frac{\vec{r}(p,k)\times d\vec{r}}{r^3(p,k)}\Gamma(k) = -\vec{n}(p)\vec{V}_\infty \tag{3}$$

In equation (3), $\vec{n}(p)$ is the "outside normal" vector to the surface S in the point *p*, with l_k identifying the semi-infinite horseshoe vortex. It is a personal contribution that the direction of every free vortex is the same with the local undisturbed velocity, $\vec{V}_{\infty i}$, composed from translation and rotation, presented in (4):

$$\vec{V}_{\infty i} = \vec{V}_\infty + \vec{\omega}\times\vec{r}_i \tag{4}$$

where $\vec{r}_i$ is the local position vector.
The numerical evaluation of the second kind Fredholm integral equation (3) relies on the approximation of integrals as follows (5):

$$2\pi\sigma_i(p) - \sum_{j=1}^{Nq}\sigma_j(q)\int_{S_j}\frac{\partial}{\partial n_i(p)}\left(\frac{1}{r(p,q)}\right)ds + \frac{1}{4\pi}\vec{n}_i(p)\sum_{k=1}^{Nk}\Gamma(k)\int_{l_k}\frac{\vec{r}(p,k)\times d\vec{r}}{r^3(p,k)} = -\vec{n}_i\vec{V}_{\infty i} \tag{5}$$

The following notations (6) present the induced velocity by a unitary sources panel from point j or by a vortex horseshoe from point k, in a collocation point i from the aircraft surface.

$$a_{ij} = \int_{S_j}\frac{\partial}{\partial n_{i(p)}}\left(\frac{1}{r(p,q)}\right)ds, \quad a_{ik} = \frac{1}{4\pi}\vec{n}_i(p)\int_{l_k}\frac{\vec{r}(p,k)\times d\vec{r}}{r(p,k)^3} \tag{6}$$

The relations (5) and (6) will give a linear algebraic equations system for the unknown σ_j and Γ_k, that are written formal in (7) as "x_j".
A robust iterative (Conjugate Gradient) solver is used for the large full matrix from (7). The results of the numerical simulations lead to the pressure coefficients and finally, by integration, to the aerodynamic coefficients and derivatives. This method was implemented "in-house" in a practical FORTRAN software code.

3. Results regarding the aerodynamic coefficients and derivatives

The aerodynamic coefficients and derivatives were evaluated with a CFD aerodynamic methodology presented in the previous chapter 2. Some numerical results were validated through those provided by a software code, Advanced Aircraft Analysis 3.3, ref [12].
The longitudinal aerodynamic coefficients and derivatives are presented in the following relations (8). There were used classical notations described in references [4] and [10].
Subscripts "F" or "S" are related to the "Full" or "Scale" models, respectively.

$$
\begin{aligned}
&C_{L0} = 0.46\,; C_{L\alpha} = 5.865\,rad^{-1}\,; \alpha_0 = -4.5\ \text{deg} \\
&C_{m0} = 0.180; C_{m\alpha} = -1.511\,rad^{-1} \\
&(C_{D0})_F = 0.0282; C_D = 0.0282 + 0.0385 C_L{}^2 \ \textit{is polar for FULL A/C} \\
&(C_{D0})_S = 0.0564; C_D = 0.0564 + 0.0385 C_L{}^2 \ \textit{is polar for SCALE A/C} \\
&C_{L\hat{q}} = 11.432\,rad^{-1}; C_{m\hat{q}} = -33.405\,rad^{-1} \\
&C_{L\dot{\alpha}} = 2.75\,rad^{-1}; C_{m\dot{\alpha}} = -11.243\,rad^{-1}
\end{aligned}
\tag{8}
$$

The aircraft HELENA has an unconventional wing and horizontal/vertical tail arrangement. This design is not suitable for lateral derivatives evaluation through classical analytical methods. Therefore, the nonlinear CFD aerodynamic model, presented in chapter 2, was used to assess the lateral-directional aerodynamic properties.
The lateral aerodynamic derivatives are given in relations (9) and summary displayed in figure 3.

$$
\begin{aligned}
&C_{y\beta} = -0.533\,rad^{-1} \\
&C_{l\beta}(C_L) = -0.0493 + 0.0735 C_L \quad \textit{is presented in figure 3} \\
&C_{n\beta}(C_L) = 0.0611 + 0.00362 C_L - 0.0403 C_L{}^2 \\
&C_{y\hat{p}} = 0.016\,rad^{-1}; C_{l\hat{p}} = -0.469\,rad^{-1}; C_{n\hat{p}} = -0.046\,rad^{-1} \\
&C_{y\hat{r}} = 0.317\,rad^{-1}; C_{l\hat{r}} = 0.109\,rad^{-1}; C_{n\hat{r}} = -0.177\,rad^{-1}
\end{aligned}
\tag{9}
$$

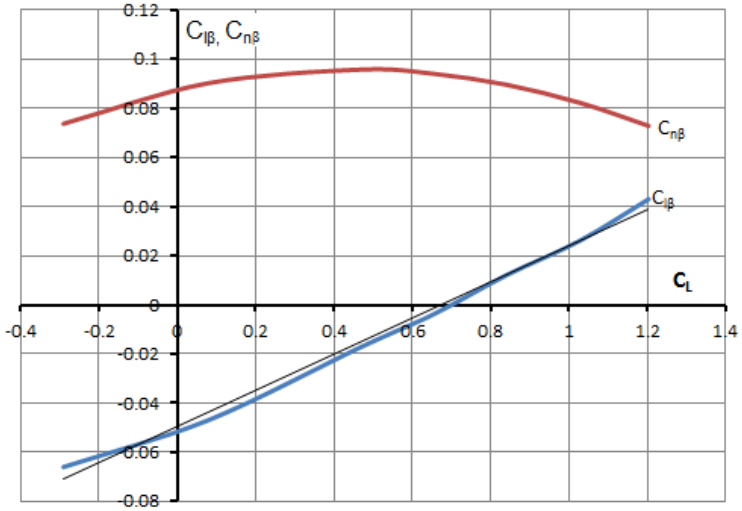

Fig.3 Rolling and Yawing derivatives versus lift coefficient C_L

The relations (9) pointed out the variation of the lateral derivatives with the lift coefficient C_L. This type of dependence is due to the interference between the wings, rear fuselage and the vertical tail and it is detailed in [4], [8], [9] and [10].

4. Aircraft Longitudinal and Lateral-Directional motion analysis

The present analysis uses the dimensional small disturbance equations system for the longitudinal and lateral directional motion, [5], [6], given through the linearization of the general motion equations. It was assumed that the motion of the airplane consists of small deviations from a reference steady symmetrical flight. The controls elevator, ailerons and rudder are kept in the fixed positions.
The longitudinal and lateral-directional dynamic system for motion analysis is formally written in (10).

$$\dot{\boldsymbol{x}} = \boldsymbol{A}\boldsymbol{x} \tag{10}$$

Hence $\boldsymbol{x}$ is the state vector and $\boldsymbol{A}$ is the system matrix. The state vectors for the longitudinal and lateral system are:

$$\boldsymbol{x} = \begin{bmatrix} \Delta u & w & q & \Delta\theta \end{bmatrix}^T \text{ for longitudinal motion} \tag{11}$$

and

$$\boldsymbol{x} = \begin{bmatrix} \beta & p & r & \Phi \end{bmatrix}^T \text{ for lateral motion,} \tag{12}$$

The $\boldsymbol{A}$ matrices from the differential system (10) are given in (13) for the longitudinal motion and in (14) for the lateral motion, respectively. These representations are based on [6] and are related to the aircraft body axis.
The state matrix for the longitudinal motion is (13):

$$\boldsymbol{A} = \begin{bmatrix} \frac{X_u}{m} & \frac{X_w}{m} & 0 & -g\cos\theta_0 \\ \frac{Z_u}{m - Z_{\dot{w}}} & \frac{Z_w}{m - Z_{\dot{w}}} & \frac{Z_q + mu_0}{m - Z_{\dot{w}}} & \frac{-mg\sin\theta_0}{m - Z_{\dot{w}}} \\ \frac{1}{I_y}\left[M_u + \frac{M_{\dot{w}} Z_u}{m - Z_{\dot{w}}}\right] & \frac{1}{I_y}\left[M_w + \frac{M_{\dot{w}} Z_w}{m - Z_{\dot{w}}}\right] & \frac{1}{I_y}\left[M_q + \frac{M_{\dot{w}}(Z_q + mu_0)}{m - Z_{\dot{w}}}\right] & \frac{-M_{\dot{w}} mg\sin\theta_0}{I_y(m - Z_{\dot{w}})} \\ 0 & 0 & 1 & 0 \end{bmatrix} \tag{13}$$

The detailed form of the dimensional longitudinal stability derivatives from (13) is a classical representation from [6] that uses the longitudinal aerodynamic coefficients and derivatives (8).
The roots of the characteristic equation $|\lambda \boldsymbol{I} - \boldsymbol{A}| = 0$ gave the eigenvalues $\lambda_{1,2SP}$ and $\lambda_{3,4PH}$. The eigenvalues $\lambda_{1,2SP}$ correspond to the short-period and $\lambda_{3,4PH}$ to the phugoid modes.
The state matrix for the lateral-directional motion is (14):

$$\boldsymbol{A} = \begin{bmatrix} \frac{Y_\beta}{mV} & \frac{Y_p}{mV} + \sin\alpha_0 & \frac{Y_r}{mV} - \cos\alpha_0 & \frac{g}{V}\cos\theta_0 \\ \frac{I_z L_\beta + I_{xz} N_\beta}{I_x I_z - I_{xz}^2} & \frac{I_z L_p + I_{xz} N_p}{I_x I_z - I_{xz}^2} & \frac{I_z L_r + I_{xz} N_r}{I_x I_z - I_{xz}^2} & 0 \\ \frac{I_x N_\beta + I_{xz} L_\beta}{I_x I_z - I_{xz}^2} & \frac{I_x N_p + I_{xz} L_p}{I_x I_z - I_{xz}^2} & \frac{I_x N_r + I_{xz} L_r}{I_x I_z - I_{xz}^2} & 0 \\ 0 & 1 & \tan\theta_0 & 0 \end{bmatrix} \tag{14}$$

The form of the lateral stability derivatives from (14) is based on the representation from [6] and uses the lateral aerodynamic derivatives (9). Usually, the roots of the lateral characteristic equation $|\lambda \boldsymbol{I} - \boldsymbol{A}| = 0$ give the eigenvalues: a conjugate complex pair $\lambda_{1,2D}$ and two real roots λ_{3R} and λ_{4S}. The complex eigenvalues $\lambda_{1,2D}$ correspond to the Dutch roll mode, a damped oscillatory motion with low frequency. The real root λ_{3R} representing a fast convergent motion is the Roll mode and λ_{4S} is the Spiral mode that may be convergent or slightly divergent.
If $\lambda_{1,2}$ is a pair of conjugate complex eigenvalues with the algebraic representation: $\lambda_{1,2} = n \pm i\omega$, the relation (15) will provide the damping ratio ς and the undamped natural circular frequency ω_n as follows:

$$\begin{aligned} &\lambda_{1,2} = -\varsigma\omega_n \pm \mathrm{i}\omega_n\sqrt{1-\varsigma^2} \\ &\text{where} \quad \varsigma = -\frac{n}{\omega_n} \text{ is damping ratio and} \\ &\qquad \omega_n = \sqrt{n^2 + \omega^2} \text{ is undamped natural frequency} \end{aligned} \tag{15}$$

The aircraft flying qualities are evaluated using the following time characteristics (16):

$$
\begin{aligned}
&Period: \quad T = \frac{2\pi}{\omega} = \frac{2\pi}{\omega_n \sqrt{1-\varsigma^2}} \\
&Time\ to\ half\ or\ double: t_{half,double} = \frac{0.693}{|n|} = \frac{0.693}{|\varsigma|\omega_n} \\
&Cycles\ to\ half\ or\ double: N_{half,double} = \frac{0.11\omega}{|n|} = \frac{0.11\sqrt{1-\varsigma^2}}{|\varsigma|} \\
&Time\ constant: \quad \tau_{R,S} = -\frac{1}{n_{R,S}} \qquad for\ nonoscillatory\ modes
\end{aligned}
\tag{16}
$$

5. Similarity criteria and aerodynamic equivalence: Full and Scale

It can be seen that the coefficients from the longitudinal and lateral state matrices $\boldsymbol{A}$ presented in (13) and (14) depends on the aircraft dimensions, inertial properties and the stability derivatives. Also the initial conditions imply a definition for aircraft velocity, V. Similarity coherent criteria are proposed for the dimensional and inertial characteristics between the real aircraft and the scale flying mock-up model. It is assumed that the linear scale factor between the real aircraft and the proposed mock-up is $SF = 20$. The table 1 presents a comparison between "Full aircraft" (F) and "Scale mock-up" (S) according to the dimensions and inertial properties.

Table 1. Similarity criteria between "Full Aircraft" and "Scale flying Mock-up"

Criteria	$(Full)_F$ Aircraft	$(Scale)_S$ Mock-up	Similarity Ratio: Scale/Full	Similarity ($SF = 20$)
Linear (e.g. span)	26 m	1.3 m	$1/SF$	1/20
Area (e.g. wing)	70 m^2	0.175 m^2	$1/SF^2$	1/400
Volume (fuselage)	179 m^3	0.0224 m^3	$1/SF^3$	1/8000
Mass (MTOW)	32000 kg	4 kg	$1/SF^3$	1/8000
Moment of inertia: I_x	336699 kgm^2	0.105 kgm^2	$1/SF^5$	1/3200000
Moment of inertia: I_y	987929 kgm^2	0.309 kgm^2	$1/SF^5$	1/3200000
Moment of inertia: I_z	1236535 kgm^2	0.386 kgm^2	$1/SF^5$	1/3200000
Moment of inertia: I_{xz}	14789 kgm^2	0.0046 kgm^2	$1/SF^5$	1/3200000
Controls deflection	The same		1	1

The similarity criteria for the inertia properties would be resolved with a specific mass distribution inside the model, assuming also the similarity for the weight. The figure 4 shows the HELENA 1/20 scale aircraft, that was developed at INCAS as a flying Radio Control mock-up, in a Wind Tunnel Testing program.

Fig 4. HELENA 1/20 scale flying mock-up in Wind Tunnel testing program

The dimensional stability derivatives from (13) and (14) are dependent by the lift coefficient C_L and the flight speed conditions, due to the representation of the dimensionless aerodynamic coefficients and derivatives from (8) and (9). For a coherent comparative analysis it is proposed that all the aerodynamic derivatives, longitudinal and lateral, appropriate to the Full aircraft and Scale flying mock-up, to be the same. This assumption implies that the lift coefficient for Full model C_{L_F} is equal to the lift coefficient for Scale model C_{L_S}, see (17):

$$C_{LF} = C_{LS} \tag{17}$$

The following relations (18), detailing the form of the lift coefficients C_{L_F} and C_{L_S}, are:

$$C_{LF} = \frac{2m_F g}{\rho S_F V_F^{\,2}} \quad , C_{LS} = \frac{2m_S g}{\rho S_S V_S^{\,2}} \tag{18}$$

Similarity criteria from table (1) and relation (18), will give, for Scale flying mock-up flight speed, V_S the form (19):

$$V_S = \sqrt{\frac{1}{SF}} \cdot V_F \tag{19}$$

where SF is the linear scale factor between Full aircraft and Scale mock-up.
The scale model has flow characteristics specific to its Reynolds number. Reynolds effects are of a great importance related to the drag properties of the scaled model. The flow, for real aircraft is at a very large Reynolds number that implies low drag properties and the flow for the scale mock-up is at low Reynolds, with penalty for drag.
This will have an effect on the longitudinal stability, especially on the Phugoid characteristics. Reynolds effects are of the second importance related to the lateral stability.
Table 2 shows the main data related to the "aerodynamic equivalence" between the flight conditions for "Full aircraft" and "Scale mock-up".

Table 2. Aerodynamic/flight conditions equivalence for "Full aircraft" and "Scale mock-up"

Flight conditions and aerodynamic coefficients	$(Full)_F$ aircraft	$(Scale)_S$ mock-up	Similarity Ratio: Scale/Full
Speed (m/s)	138	30.8	$\sqrt{1/SF}$
Mean aerodynamic chord	3.11	0.155	$1/SF$
Re	29.4 10^6	329000	$1/(SF)^{3/2}$
Lift Coefficient C_L	0.388	0.388	1
Drag Coefficient C_{D0}	0.0282	0.0564	2, for this case
Lateral aerodynamic derivatives (8)	The same		1
Lateral rotary derivatives (9)	The same		1

6. Longitudinal modes, "Full aircraft" and "Scale mock-up" comparison

The analysis for the longitudinal and lateral stability, appropriate to the "Full" aircraft and "Scale" mock-up, was made according to the similarity criteria detailed in Table 1 and the aerodynamic equivalence from Table 2. The steady straight flight level is assumed to be the reference condition for both airplanes models.
A numerical integration method, Runke-Kutta of 4-th order from Mathcad was used to evaluate the solutions of the system (10), for Full aircraft and Scale mock-up. The eigenvalues and eigenvectors were processed.
The longitudinal motion analysis has, as input data, the state matrices A_F for Full aircraft, and A_S for Scale mock-up. These are given in (20).

$$A_F = \begin{pmatrix} -0.017 & 0.056 & 0 & -9.81 \\ -0.155 & -1.075 & 133.858 & 0.086 \\ 8.424\times 10^{-4} & -0.025 & -1.273 & -2.016\times 10^{-4} \\ 0 & 0 & 1 & 0 \end{pmatrix}, \qquad A_S = \begin{pmatrix} -0.144 & 0.251 & 0 & -9.81 \\ -0.691 & -4.83 & 29.932 & 0.086 \\ 0.075 & -2.27 & -5.695 & -4.032\times 10^{-3} \\ 0 & 0 & 1 & 0 \end{pmatrix}, \tag{20}$$

The eigenvalues λ_F for Full aircraft and λ_S for Scale mock-up become (21):

$$\lambda_F = \begin{pmatrix} -1.175+1.841i \\ -1.175-1.841i \\ -7.547\times 10^{-3}+0.099i \\ -7.547\times 10^{-3}-0.099i \end{pmatrix}, \text{ for Full aircraft} \qquad \lambda_S = \begin{pmatrix} -5.266+8.233i \\ -5.266-8.233i \\ -0.068+0.441i \\ -0.068-0.441i \end{pmatrix}, \text{ for Scale mock-up} \tag{21}$$

According to the real parts of the eigenvalues from (21), the longitudinal modes, Short period and Phugoid mode are seen to be stable.
Due to the similarity criteria and the aerodynamic equivalence, relation (22) shows the dependence between the eigenvalues λ_F and λ_S for the Short period mode as follows:

$$\lambda_F = \lambda_S / \sqrt{SF} \quad or \quad \lambda_F = \lambda_S / \sqrt{20} \tag{22}$$

A numerical study related to the sensitivity of the phugoid damping factor $(\xi_S)_{ph}$ at the aerodynamic drag coefficient CD_{0S} is presented in table 3. The range of the drag coefficient was "formal" assumed at 282…846 counts.

Table 3. Phugoid damping sensitivity at the "Scale" aerodynamic drag

CD_{0S}	$(\zeta_S)_{ph}$	$(\zeta_S/\zeta_F)_{ph}$	CD_{0S}/CD_{0F}	$(t_{half\ S})_{ph}$	$(t_{half\ F})^*_{ph}$	$(t_{half\ F})_{ph}$
0.0282	0.076	1	1	20.53	91.81	
0.0423	0.115	1.513	1.5	13.568	91.01	
0.0564	0.153	2.013	2	10.149	90.78	91.827
0.0705	0.192	2.52	2.5	8.083	90.4	
0.0846	0.231	3.04	3	6.724	90.2	

where	CD_{0F}=	0.0282
	$(\zeta_F)_{ph}$=	0.076
	$(t_{half\ F})_{ph}$=	91.827

The numerical results from Table 3 shows a quasi-linear dependency between the damping factor $(\xi_S)_{ph}$ and the aerodynamic drag coefficient CD_{0S} This is given in relation (23).

$$\left(\frac{\zeta_S}{\zeta_F}\right)_{ph} \cong \left(\frac{CD_{0S}}{CD_{0F}}\right) \tag{23}$$

The value $(t_{half\ F})^*_{ph}$ from table 3 was evaluated according to relation (24), that takes into account the similarity criteria and the aerodynamic equivalence.

$$(t_{halfF})^*_{ph} = (t_{halfS})_{ph}\sqrt{SF}\left(\frac{CD_{0S}}{CD_{0F}}\right) \tag{24}$$

It can be seen a close agreement between the exact value of the time to half $(t_{halfF})_{ph}$ and the proposed value $(t_{halfF})^*_{ph}$ given by (24).

Table 4 shows a comparison for the longitudinal characteristics times and damping ratio for the Full aircraft and Scale mock-up.

Table 4. Characteristics Times-Longitudinal Modes

M O D E		$(Scale)_S$ mock-up	$(Full)_F$ aircraft	SIMILARITY ($SF = 20$)
Short period mode (damped oscillation)	ξ	0.538	0.538	$\xi_F = \xi_S$
	ω_n	9.733	2.184	$\omega_{nF} = \omega_{nS} / \sqrt{SF}$
	T	0.763	3.41	$T_F = T_S \sqrt{SF}$
	t_{half}	0.132	0.59	$t_{half_F} = t_{half_S} \sqrt{SF}$
	N_{half}	0.172	0.172	$N_{half_F} = N_{half_S}$
Phugoid mode (damped oscillation)	C_{D0}	0.0564	0.0280	$C_{D0S} / C_{D0F} = 2$
	ξ	0.153	0.076	$\varsigma_F \cong \varsigma_S (\frac{CD_{0F}}{CD_{0S}})$
	ω_n	0.446	0.1	$\omega_{nF} = \omega_{nS} / \sqrt{SF}$
	T	14.26	63.21	$T_F = T_S \sqrt{SF}$
	t_{half}	10.149	91.827	$t_{halfF} \cong t_{halfS} \sqrt{SF} (\frac{CD_{0S}}{CD_{0F}})$
	N_{half}	0.712	0.712	$N_{half_F} = N_{half_S}$

The figures from Table 4 confirm the assumptions from relations (23) and (24) and have good qualitative and quantitative values.
The transient behaviour of the state variables in the longitudinal motion, for Short period mode, is displayed in figure 5 .

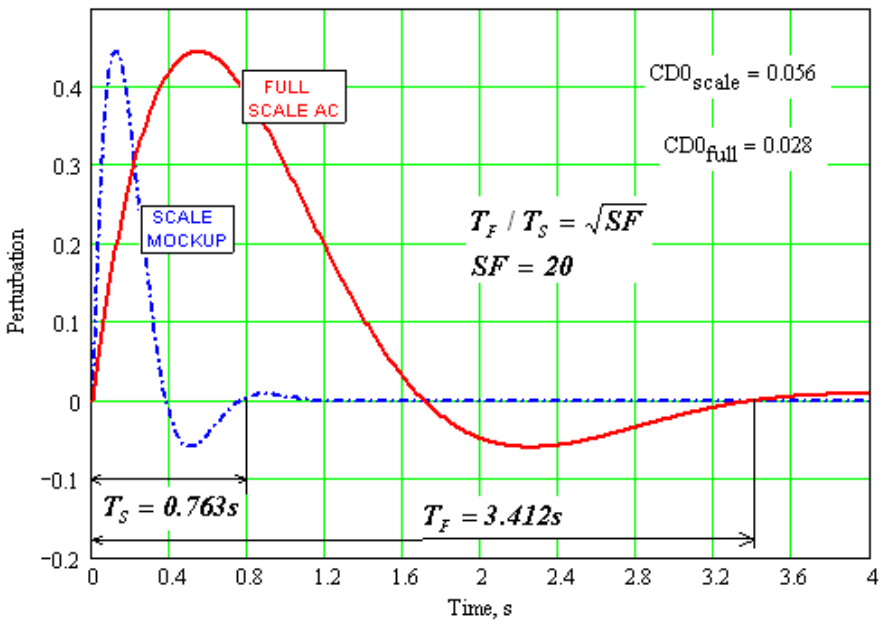

Figure 5. Characteristics transient, Short period mode

The transient behaviour of the state variables in the longitudinal motion for Phugoid mode is displayed in figure 6.

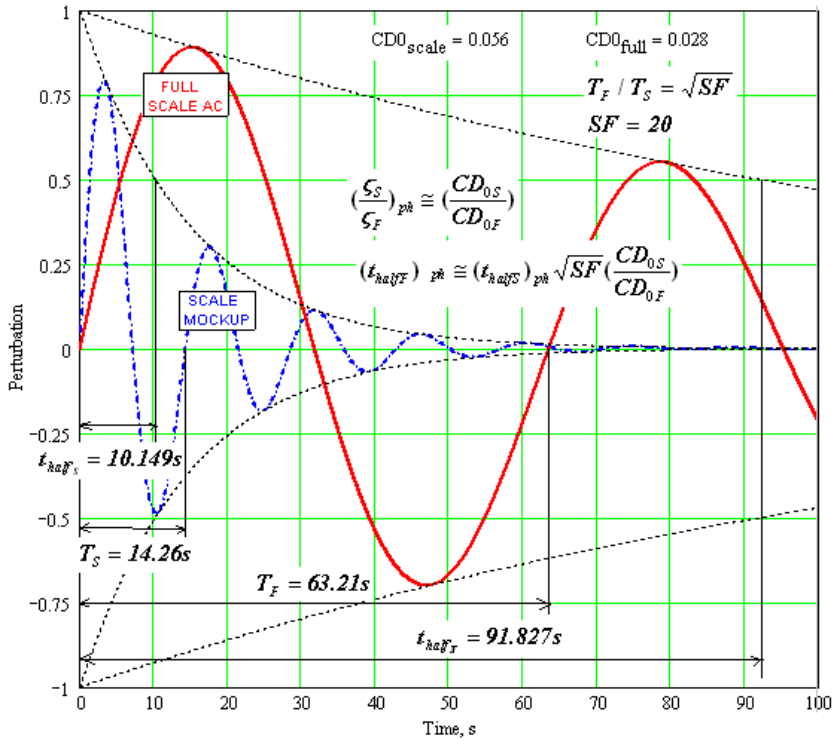

Figure 6. Characteristics transient, Phugoid mode

7. Lateral modes, "Full aircraft" and "Scale mock-up" comparison

The lateral-directional motion analysis has, as input data, the state matrices A_F for Full aircraft, and A_S for Scale mock-up. These are given in (25).

$$A_F = \begin{pmatrix} -0.0977 & -0.0130 & -0.9944 & 0.0711 \\ -1.1565 & -2.7604 & 0.6324 & 0.0000 \\ 1.6980 & -0.1065 & -0.2771 & 0.0000 \\ 0.0000 & 1.0000 & -0.0112 & 0.0000 \end{pmatrix}, \quad A_S = \begin{pmatrix} -0.4370 & -0.0130 & -0.9944 & 0.3182 \\ -23.1303 & -12.3448 & 2.8283 & 0.0000 \\ 33.9598 & -0.4762 & -1.2390 & 0.0000 \\ 0.0000 & 1.0000 & -0.0112 & 0.0000 \end{pmatrix}, \tag{25}$$

The eigenvalues λ_F for Full aircraft and λ_S for Scale mock-up become (26):

$$\lambda_F = \begin{pmatrix} -0.1867 + 1.3282i \\ -0.1867 - 1.3282i \\ -2.7718 \\ 0.0100 \end{pmatrix}, \text{ for Full aircraft} \qquad \lambda_S = \begin{pmatrix} -0.8348 + 5.9400i \\ -0.8348 - 5.9400i \\ -12.3958 \\ 0.0446 \end{pmatrix}, \text{ for Scale Mock-up} \tag{26}$$

The first two modes are seen to be stable. The first mode is a damped oscillation, Dutch Roll. The second, Roll mode, is aperiodic very rapid convergent. The third mode, Spiral mode is very slow aperiodic divergent.
Due to the similarity criteria and the aerodynamic equivalence, relation (22) that shows the dependence of the eigenvalues between λ_F and λ_S remains valid for all the lateral modes.
The above similarity criteria become an invariant for the eigenvalues, if the lateral-directional analysis is made using NACA Dimensionless System [4].
Using this technique will lead to the same eigenvalues λ_S and λ_F. In this case the dimensionless time constants t_F^* for Full aircraft and t_S^* for Scale mock-up are in relation (27):

$$t_F^* = \sqrt{SF}\, t_S^* \quad or \quad t_F^* = \sqrt{20}\, t_S^* \tag{27}$$

Table 5 shows a comparison for the characteristics times and damping ratio of the Full aircraft and Scale mock-up in the lateral-directional motion analysis.

Table 5. Characteristics Times-Lateral Modes

M O D E		$(Scale)_S$ mock-up	$(Full)_F$ aircraft	SIMILARITY ($SF = 20$)
Dutch Roll (damped oscillation)	ξ	0.139	0.139	$\xi_F = \xi_S$
	ω_n	5.998	1.341	$\omega_{nF} = \omega_{nS} / \sqrt{SF}$
	T	1.058	4.73	$T_F = T_S \sqrt{SF}$
	t_{half}	0.830	3.71	$t_{half_F} = t_{half_S} \sqrt{SF}$
	N_{half}	0.783	0.783	$N_{half_F} = N_{half_S}$
Roll (convergent)	τ	0.0807	0.361	$\tau_F = \tau_S \sqrt{SF}$
	t_{half}	0.0559	0.250	$t_{half_F} = t_{half_S} \sqrt{SF}$
Spiral (divergent)	τ	-22.4	-100.21	$\tau_F = \tau_S \sqrt{SF}$
	t_{double}	15.53	69.46	$t_{half_F} = t_{half_S} \sqrt{SF}$

The results from table 3 show the same damping ratio and cycles in Dutch Roll mode.
The time characteristics for the Full aircraft are obtained from those of the Scale mock-up multiplied with a constant, $\sqrt{SF}$. The transient behaviour of the state variables in the lateral-directional motion is displayed in figure 7 for the Dutch Roll mode, in figure 8 for the Roll mode and in figure 9 for the Spiral mode, respectively.

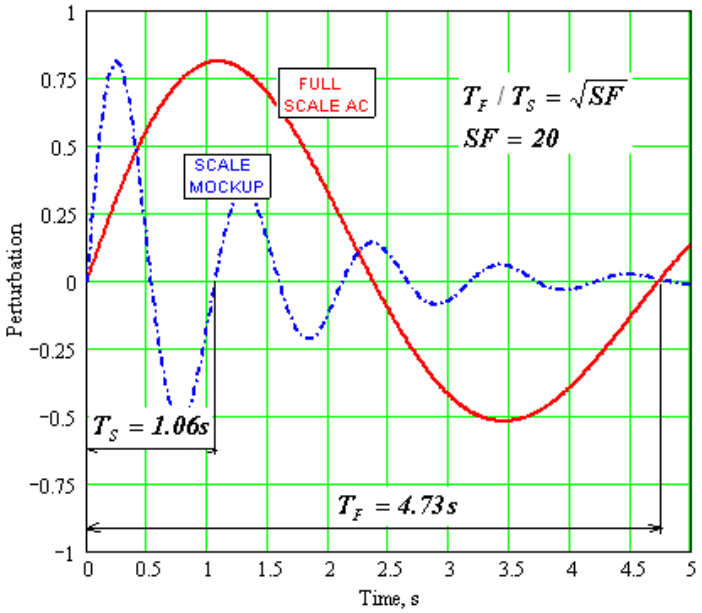

Figure 7. Characteristics transient, Dutch Roll mode

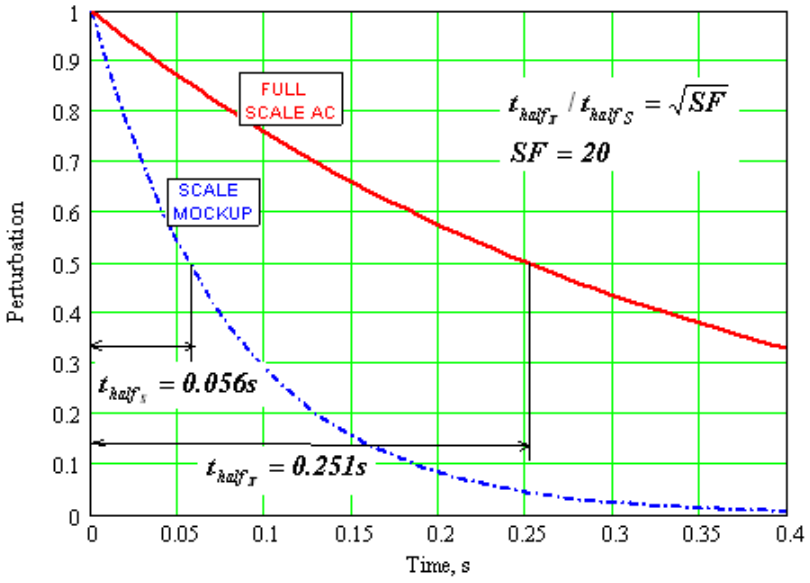

Figure 8. Characteristics transient, Roll mode

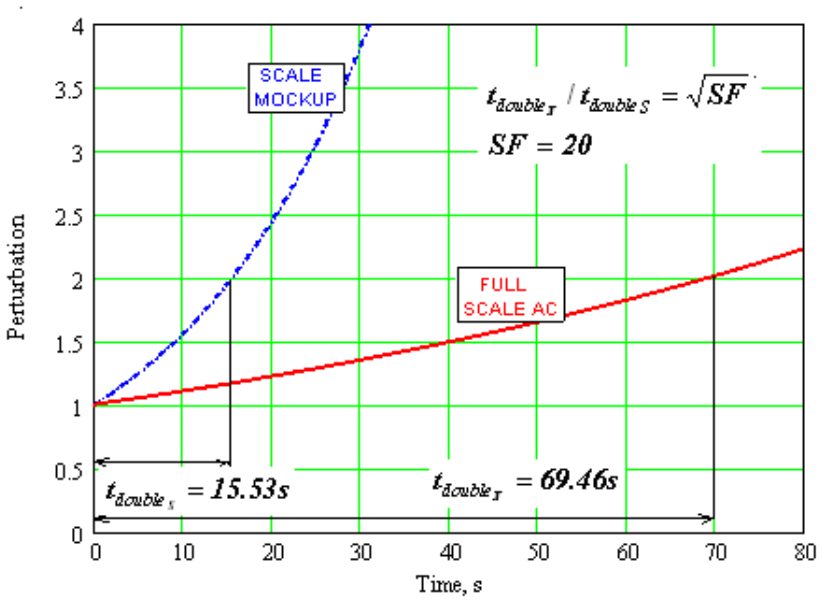

Figure 9. Characteristics transitent, Spiral mode

8. Conclusions

This specific analysis about longitudinal and lateral-directional aircraft stability details how to translate, in a coherent mode, the results from a “scale flying mock-up” to the “full aircraft”.

A practical “in-house” aerodynamic “boundary element” model was developed and used to evaluate the longitudinal and lateral aerodynamic coefficients and their stability derivatives.

There are proposed similarity coherent criteria for the dimensional, inertial and mass characteristics between the real aircraft and the scale mock-up model.

The equivalence for the aerodynamic derivatives for the real aircraft and the scale mock-up is achieved by choosing a flight regime that preserves the lift coefficient.

Longitudinal stability analysis for the real aircraft and the scale model plane shows the same values for the damping factor in "Short period mode" and factored value with a scale constant for the time characteristics.

The damping ratio in phugoid mode for scale model and full aircraft seems to be proportional to the aerodynamic drag ratio of the two models.

The comparison between the real aircraft and the scale model plane shows the same values for the damping factor in "Dutch roll".

Factored values with a scale constant are obtained for the time characteristics in "Dutch roll", “Roll” and “Spiral” modes.

References

[1] *S. Bogos, D. Turcanu*, The Aerodynamic and Dynamic Ventral Fins Effects on a Jet Trainer, 22nd Congress of International Council of the Aeronautical Sciences, Harrogate, UK, 2000, Paper ICAS 2000-2.1.4

[2] *Brad A. Seanor,* Flight Testing of a Remotely Piloted Vehicle for Aircraft Parameter Estimation Purposes, Dissertation for the degree of PhD in Aerospace Engineering, Morgantown, West Virginia, 2002

[3] *S. Bogos, I. Stroe*, Similarity Criteria for “Full” and “Scale” Aircraft on the Lateral Stability Analysis, U.P.B Sci. Bull., Series D, Vol. 74, Iss. 4, 2012, ISSN 1454-2358

[4] *Etkin B.* Dynamics of Flight-Stability and Control. John Wiley & Sons, NY, 1959

[5] *Etkin B.* Dynamics of Atmospheric Flight, John Wiley & Sons , NY, 1972

[6] *Etkin B., Reid L. D.*, Dynamics of Flight-Stability and Control, Third Edition, John Wiley & Sons, NY, 1996

[7] *Hess J. L., Smith A. M. O.,* Calculation of Potential Flow about arbitrary bodies, Progress in Aeronautical Sciences, Vol. 8, 1967

[8] *Perkins C. D.,Hage R. E.,* Airplane Performance Stability and Control, John Wiley & Sons, NY, 1967

[9] *Lan C. T., Roskam J.,* Airplane Aerodynamics and Performance, DAR Corporation, 2003

[10] *Roskam J.,* Airplane Flight Dynamics and Automatic Flight Controls, Part I and II, DAR Corporation, 2003

[11] *M. Hepperle*, MDO of Forward Swept Wings, KATnet II Workshop, January 2008, Braunschweig

[12] *D A R Corporation*, Advanced Aircraft Analysis software v 3.3, 2011.